

Evidence for $\eta_c(2S)$ in $\psi(3686) \rightarrow \gamma K_S^0 K^\pm \pi^\mp \pi^+ \pi^-$

3 M. Ablikim¹, M. N. Achasov⁶, O. Albayrak³, D. J. Ambrose³⁹, F. F. An¹, Q. An⁴⁰, J. Z. Bai¹,
 4 R. Baldini Ferroli^{17A}, Y. Ban²⁶, J. Becker², J. V. Bennett¹⁶, M. Bertani^{17A}, J. M. Bian³⁸,
 5 E. Boger^{19,a}, O. Bondarenko²⁰, I. Boyko¹⁹, R. A. Briere³, V. Bytev¹⁹, H. Cai⁴⁴, X. Cai¹,
 6 O. Cakir^{34A}, A. Calcaterra^{17A}, G. F. Cao¹, S. A. Cetin^{34B}, J. F. Chang¹, G. Chelkov^{19,a},
 7 G. Chen¹, H. S. Chen¹, J. C. Chen¹, M. L. Chen¹, S. J. Chen²⁴, X. Chen²⁶, Y. B. Chen¹,
 8 H. P. Cheng¹⁴, Y. P. Chu¹, D. Cronin-Hennessy³⁸, H. L. Dai¹, J. P. Dai¹, D. Dedovich¹⁹,
 9 Z. Y. Deng¹, A. Denig¹⁸, I. Denysenko^{19,b}, M. Destefanis^{43A,43C}, W. M. Ding²⁸, Y. Ding²²,
 10 L. Y. Dong¹, M. Y. Dong¹, S. X. Du⁴⁶, J. Fang¹, S. S. Fang¹, L. Fava^{43B,43C}, C. Q. Feng⁴⁰,
 11 P. Friedel², C. D. Fu¹, J. L. Fu²⁴, Y. Gao³³, C. Geng⁴⁰, K. Goetzen⁷, W. X. Gong¹, W. Gradl¹⁸,
 12 M. Greco^{43A,43C}, M. H. Gu¹, Y. T. Gu⁹, Y. H. Guan³⁶, A. Q. Guo²⁵, L. B. Guo²³, T. Guo²³,
 13 Y. P. Guo²⁵, Y. L. Han¹, F. A. Harris³⁷, K. L. He¹, M. He¹, Z. Y. He²⁵, T. Held², Y. K. Heng¹,
 14 Z. L. Hou¹, C. Hu²³, H. M. Hu¹, J. F. Hu³⁵, T. Hu¹, G. M. Huang⁴, G. S. Huang⁴⁰,
 15 J. S. Huang¹², L. Huang¹, X. T. Huang²⁸, Y. Huang²⁴, Y. P. Huang¹, T. Hussain⁴², C. S. Ji⁴⁰,
 16 Q. Ji¹, Q. P. Ji²⁵, X. B. Ji¹, X. L. Ji¹, L. L. Jiang¹, X. S. Jiang¹, J. B. Jiao²⁸, Z. Jiao¹⁴,
 17 D. P. Jin¹, S. Jin¹, F. F. Jing³³, N. Kalantar-Nayestanaki²⁰, M. Kavatsyuk²⁰, B. Kopf²,
 18 M. Kornicer³⁷, W. Kuehn³⁵, W. Lai¹, J. S. Lange³⁵, M. Leyhe², C. H. Li¹, Cheng Li⁴⁰, Cui Li⁴⁰,
 19 D. M. Li⁴⁶, F. Li¹, G. Li¹, H. B. Li¹, J. C. Li¹, K. Li¹⁰, Lei Li¹, Q. J. Li¹, S. L. Li¹, W. D. Li¹,
 20 W. G. Li¹, X. L. Li²⁸, X. N. Li¹, X. Q. Li²⁵, X. R. Li²⁷, Z. B. Li³², H. Liang⁴⁰, Y. F. Liang³⁰,
 21 Y. T. Liang³⁵, G. R. Liao³³, X. T. Liao¹, D. Lin¹¹, B. J. Liu¹, C. L. Liu³, C. X. Liu¹, F. H. Liu²⁹,
 22 Fang Liu¹, Feng Liu⁴, H. Liu¹, H. B. Liu⁹, H. H. Liu¹³, H. M. Liu¹, H. W. Liu¹, J. P. Liu⁴⁴,
 23 K. Liu³³, K. Y. Liu²², Kai Liu³⁶, P. L. Liu²⁸, Q. Liu³⁶, S. B. Liu⁴⁰, X. Liu²¹, Y. B. Liu²⁵,
 24 Z. A. Liu¹, Zhiqiang Liu¹, Zhiqing Liu¹, H. Loehner²⁰, G. R. Lu¹², H. J. Lu¹⁴, J. G. Lu¹,
 25 Q. W. Lu²⁹, X. R. Lu³⁶, Y. P. Lu¹, C. L. Luo²³, M. X. Luo⁴⁵, T. Luo³⁷, X. L. Luo¹, M. Lv¹,
 26 C. L. Ma³⁶, F. C. Ma²², H. L. Ma¹, Q. M. Ma¹, S. Ma¹, T. Ma¹, X. Y. Ma¹, F. E. Maas¹¹,
 27 M. Maggiora^{43A,43C}, Q. A. Malik⁴², Y. J. Mao²⁶, Z. P. Mao¹, J. G. Messchendorp²⁰,
 28 J. Min¹, T. J. Min¹, R. E. Mitchell¹⁶, X. H. Mo¹, C. Morales Morales¹¹, N. Yu. Muchnoi⁶,
 29 H. Muramatsu³⁹, Y. Nefedov¹⁹, C. Nicholson³⁶, I. B. Nikolaev⁶, Z. Ning¹, S. L. Olsen²⁷,
 30 Q. Ouyang¹, S. Pacetti^{17B}, J. W. Park²⁷, M. Pelizaeus², H. P. Peng⁴⁰, K. Peters⁷, J. L. Ping²³,
 31 R. G. Ping¹, R. Poling³⁸, E. Prencipe¹⁸, M. Qi²⁴, S. Qian¹, C. F. Qiao³⁶, L. Q. Qin²⁸, X. S. Qin¹,
 32 Y. Qin²⁶, Z. H. Qin¹, J. F. Qiu¹, K. H. Rashid⁴², G. Rong¹, X. D. Ruan⁹, A. Sarantsev^{19,c},
 33 B. D. Schaefer¹⁶, M. Shao⁴⁰, C. P. Shen^{37,d}, X. Y. Shen¹, H. Y. Sheng¹, M. R. Shepherd¹⁶,
 34 X. Y. Song¹, S. Spataro^{43A,43C}, B. Spruck³⁵, D. H. Sun¹, G. X. Sun¹, J. F. Sun¹², S. S. Sun¹,
 35 Y. J. Sun⁴⁰, Y. Z. Sun¹, Z. J. Sun¹, Z. T. Sun⁴⁰, C. J. Tang³⁰, X. Tang¹, I. Tapan^{34C},
 36 E. H. Thorndike³⁹, D. Toth³⁸, M. Ullrich³⁵, I. U. Uman^{34A,e}, G. S. Varner³⁷, B. Q. Wang²⁶,
 37 D. Wang²⁶, D. Y. Wang²⁶, K. Wang¹, L. L. Wang¹, L. S. Wang¹, M. Wang²⁸, P. Wang¹,
 38 P. L. Wang¹, Q. J. Wang¹, S. G. Wang²⁶, X. F. Wang³³, X. L. Wang⁴⁰, Y. D. Wang^{17A},
 39 Y. F. Wang¹, Y. Q. Wang¹⁸, Z. Wang¹, Z. G. Wang¹, Z. Y. Wang¹, D. H. Wei⁸, J. B. Wei²⁶,
 40 P. Weidenkaff¹⁸, Q. G. Wen⁴⁰, S. P. Wen¹, M. Werner³⁵, U. Wiedner², L. H. Wu¹, N. Wu¹,
 41 S. X. Wu⁴⁰, W. Wu²⁵, Z. Wu¹, L. G. Xia³³, Y. X. Xia¹⁵, Z. J. Xiao²³, Y. G. Xie¹, Q. L. Xiu¹,
 42 G. F. Xu¹, G. M. Xu²⁶, Q. J. Xu¹⁰, Q. N. Xu³⁶, X. P. Xu³¹, Z. R. Xu⁴⁰, F. Xue⁴, Z. Xue¹,
 43 L. Yan⁴⁰, W. B. Yan⁴⁰, Y. H. Yan¹⁵, H. X. Yang¹, Y. Yang⁴, Y. X. Yang⁸, H. Ye¹, M. Ye¹,

44 M. H. Ye⁵, B. X. Yu¹, C. X. Yu²⁵, H. W. Yu²⁶, J. S. Yu²¹, S. P. Yu²⁸, C. Z. Yuan¹, Y. Yuan¹,
45 A. A. Zafar⁴², A. Zallo^{17A}, Y. Zeng¹⁵, B. X. Zhang¹, B. Y. Zhang¹, C. Zhang²⁴, C. C. Zhang¹,
46 D. H. Zhang¹, H. H. Zhang³², H. Y. Zhang¹, J. Q. Zhang¹, J. W. Zhang¹, J. Y. Zhang¹,
47 J. Z. Zhang¹, LiLi Zhang¹⁵, R. Zhang³⁶, S. H. Zhang¹, X. J. Zhang¹, X. Y. Zhang²⁸, Y. Zhang¹,
48 Y. H. Zhang¹, Z. P. Zhang⁴⁰, Z. Y. Zhang⁴⁴, Zhenghao Zhang⁴, G. Zhao¹, H. S. Zhao¹,
49 J. W. Zhao¹, K. X. Zhao²³, Lei Zhao⁴⁰, Ling Zhao¹, M. G. Zhao²⁵, Q. Zhao¹, Q. Z. Zhao⁹,
50 S. J. Zhao⁴⁶, T. C. Zhao¹, X. H. Zhao²⁴, Y. B. Zhao¹, Z. G. Zhao⁴⁰, A. Zhemchugov^{19,a},
51 B. Zheng⁴¹, J. P. Zheng¹, Y. H. Zheng³⁶, B. Zhong²³, Z. Zhong⁹, L. Zhou¹, X. Zhou⁴⁴,
52 X. K. Zhou³⁶, X. R. Zhou⁴⁰, C. Zhu¹, K. Zhu¹, K. J. Zhu¹, S. H. Zhu¹, X. L. Zhu³³,
53 Y. C. Zhu⁴⁰, Y. M. Zhu²⁵, Y. S. Zhu¹, Z. A. Zhu¹, J. Zhuang¹, B. S. Zou¹, J. H. Zou¹

54 (BESIII Collaboration)

55 ¹ *Institute of High Energy Physics, Beijing 100049, People's Republic of China*

56 ² *Bochum Ruhr-University, D-44780 Bochum, Germany*

57 ³ *Carnegie Mellon University, Pittsburgh, Pennsylvania 15213, USA*

58 ⁴ *Central China Normal University, Wuhan 430079, People's Republic of China*

59 ⁵ *China Center of Advanced Science and Technology, Beijing 100190, People's Republic of China*

60 ⁶ *G.I. Budker Institute of Nuclear Physics SB RAS (BINP), Novosibirsk 630090, Russia*

61 ⁷ *GSI Helmholtzcentre for Heavy Ion Research GmbH, D-64291 Darmstadt, Germany*

62 ⁸ *Guangxi Normal University, Guilin 541004, People's Republic of China*

63 ⁹ *GuangXi University, Nanning 530004, People's Republic of China*

64 ¹⁰ *Hangzhou Normal University, Hangzhou 310036, People's Republic of China*

65 ¹¹ *Helmholtz Institute Mainz, Johann-Joachim-Becher-Weg 45, D-55099 Mainz, Germany*

66 ¹² *Henan Normal University, Xinxiang 453007, People's Republic of China*

67 ¹³ *Henan University of Science and Technology, Luoyang 471003, People's Republic of China*

68 ¹⁴ *Huangshan College, Huangshan 245000, People's Republic of China*

69 ¹⁵ *Hunan University, Changsha 410082, People's Republic of China*

70 ¹⁶ *Indiana University, Bloomington, Indiana 47405, USA*

71 ¹⁷ *(A)INFN Laboratori Nazionali di Frascati, I-00044, Frascati,*

72 *Italy; (B)INFN and University of Perugia, I-06100, Perugia, Italy*

73 ¹⁸ *Johannes Gutenberg University of Mainz,*

74 *Johann-Joachim-Becher-Weg 45, D-55099 Mainz, Germany*

75 ¹⁹ *Joint Institute for Nuclear Research, 141980 Dubna, Moscow region, Russia*

76 ²⁰ *KVI, University of Groningen, NL-9747 AA Groningen, The Netherlands*

77 ²¹ *Lanzhou University, Lanzhou 730000, People's Republic of China*

78 ²² *Liaoning University, Shenyang 110036, People's Republic of China*

79 ²³ *Nanjing Normal University, Nanjing 210023, People's Republic of China*

80 ²⁴ *Nanjing University, Nanjing 210093, People's Republic of China*

81 ²⁵ *Nankai University, Tianjin 300071, People's Republic of China*

82 ²⁶ *Peking University, Beijing 100871, People's Republic of China*

83 ²⁷ *Seoul National University, Seoul, 151-747 Korea*

84 ²⁸ *Shandong University, Jinan 250100, People's Republic of China*

85 ²⁹ *Shanxi University, Taiyuan 030006, People's Republic of China*

86 ³⁰ *Sichuan University, Chengdu 610064, People's Republic of China*

87 ³¹ *Soochow University, Suzhou 215006, People's Republic of China*

88 ³² *Sun Yat-Sen University, Guangzhou 510275, People's Republic of China*

89
90
91
92
93
94
95
96
97
98
99
100
101
102
103
104
105
106
107
108
109

- ³³ *Tsinghua University, Beijing 100084, People's Republic of China*
- ³⁴ (A) *Ankara University, Dogol Caddesi, 06100 Tandogan, Ankara, Turkey; (B) Dogus University, 34722 Istanbul, Turkey; (C) Uludag University, 16059 Bursa, Turkey*
- ³⁵ *Universitaet Giessen, D-35392 Giessen, Germany*
- ³⁶ *University of Chinese Academy of Sciences, Beijing 100049, People's Republic of China*
- ³⁷ *University of Hawaii, Honolulu, Hawaii 96822, USA*
- ³⁸ *University of Minnesota, Minneapolis, Minnesota 55455, USA*
- ³⁹ *University of Rochester, Rochester, New York 14627, USA*
- ⁴⁰ *University of Science and Technology of China, Hefei 230026, People's Republic of China*
- ⁴¹ *University of South China, Hengyang 421001, People's Republic of China*
- ⁴² *University of the Punjab, Lahore-54590, Pakistan*
- ⁴³ (A) *University of Turin, I-10125, Turin, Italy; (B) University of Eastern Piedmont, I-15121, Alessandria, Italy; (C) INFN, I-10125, Turin, Italy*
- ⁴⁴ *Wuhan University, Wuhan 430072, People's Republic of China*
- ⁴⁵ *Zhejiang University, Hangzhou 310027, People's Republic of China*
- ⁴⁶ *Zhengzhou University, Zhengzhou 450001, People's Republic of China*
- ^a *Also at the Moscow Institute of Physics and Technology, Moscow 141700, Russia*
- ^b *On leave from the Bogolyubov Institute for Theoretical Physics, Kiev 03680, Ukraine*
- ^c *Also at the PNPI, Gatchina 188300, Russia*
- ^d *Present address: Nagoya University, Nagoya 464-8601, Japan*
- ^e *Currently at: Dogus University, Istanbul, Turkey*

Abstract

We search for the M1 radiative transition $\psi(3686) \rightarrow \gamma\eta_c(2S)$ by reconstructing the exclusive $\eta_c(2S) \rightarrow K_S^0 K^\pm \pi^\mp \pi^+ \pi^-$ decay using 1.06×10^8 $\psi(3686)$ events collected with the BESIII detector. The signal is observed with a statistical significance of greater than 4 standard deviations. The measured mass of the $\eta_c(2S)$ is $3646.9 \pm 1.6(\text{stat}) \pm 3.6(\text{syst}) \text{ MeV}/c^2$, and the width is $9.9 \pm 4.8(\text{stat}) \pm 2.9(\text{syst}) \text{ MeV}/c^2$. The product branching fraction is measured to be $\mathcal{B}(\psi(3686) \rightarrow \gamma\eta_c(2S)) \times \mathcal{B}(\eta_c(2S) \rightarrow K_S^0 K^\pm \pi^\mp \pi^+ \pi^-) = (7.03 \pm 2.10(\text{stat}) \pm 0.70(\text{syst})) \times 10^{-6}$. This measurement complements a previous BESIII measurement of $\psi(3686) \rightarrow \gamma\eta_c(2S)$ with $\eta_c(2S) \rightarrow K_S^0 K^\pm \pi^\mp$ and $K^+ K^- \pi^0$.

110 PACS numbers: 13.20.Gd, 13.25.Gv, 14.40.Pq

I. INTRODUCTION

Compared to other charmonium states with masses below the open charm threshold, the properties of the $\eta_c(2S)$ are not well-established. The determination of the $\eta_c(2S)$ mass, in particular, provides useful information about the spin-spin part of the charmonium potential. The $\eta_c(2S)$ was first observed at B -factories [1–4] and, to date, the only two measured branching fractions are for decays to $K\bar{K}\pi$ and $K^+K^-\pi^+\pi^-\pi^0$ [5]. While the absolute branching fractions currently have poor precision, BaBar used the two-photon fusion process to measure the ratio of $\mathcal{B}(\eta_c(2S) \rightarrow K^+K^-\pi^+\pi^-\pi^0)$ to $\mathcal{B}(\eta_c(2S) \rightarrow K_S^0K^\pm\pi^\mp)$ to be $2.2 \pm 0.5(\text{stat}) \pm 0.5(\text{syst})$ [6]. The production of the $\eta_c(2S)$ is also expected from magnetic dipole (M1) transitions [7] of the $\psi(3686)$, and $\psi(3686) \rightarrow \gamma\eta_c(2S)$ with $\eta_c(2S) \rightarrow K\bar{K}\pi$ has previously been observed by BESIII [8]. This analysis complements the previous analysis by focusing on the same radiative decay, $\psi(3686) \rightarrow \gamma\eta_c(2S)$, but with $\eta_c(2S) \rightarrow K_S^0K^\pm\pi^\mp\pi^+\pi^-$.

In our study, $\psi(3686)$ mesons are produced by the annihilation of electron-positron pairs at a center-of-mass energy of 3686 MeV. The production of the $\eta_c(2S)$ through a radiative transition from the $\psi(3686)$ requires a charmed-quark spin-flip and, thus, proceeds via a M1 transition. Some of the generated $\eta_c(2S)$ mesons will decay into hadrons, and then ultimately into detectable particles, like pions, kaons, and photons. We study the decay exclusively by reconstructing the $\eta_c(2S)$ from its hadronic decay products and analyze the $\eta_c(2S)$ candidate mass for an evidence of $\psi(3686) \rightarrow \gamma\eta_c(2S)$. The experimental challenge of the measurement of this decay channel is to detect the 48 MeV radiative photons in an experimental environment with considerable backgrounds, therefore the success of this study depends on a careful and detailed analysis of all possible background sources.

II. THE EXPERIMENT AND DATA SETS

The data sample for this analysis consists of 1.06×10^8 events produced at the peak of the $\psi(3686)$ resonance [9]. Data were collected with an additional integrated luminosity of 42 pb^{-1} at a center-of-mass energy of $\sqrt{s}=3.65 \text{ GeV}$ to determine non-resonant continuum background contributions. The data were accumulated with the BESIII detector operated at the BEPCII e^+e^- collider.

The BESIII detector, described in detail in Ref. [10], has an effective geometrical acceptance of 93% of 4π . It contains a small cell helium-based main drift chamber (MDC) which provides momentum measurements of charged particles; a time-of-flight system (TOF) based on plastic scintillator which helps to identify charged particles; an electromagnetic calorimeter (EMC) made of CsI (Tl) crystals which is used to measure the energies of photons and provide trigger signals; and a muon system (MUC) made of Resistive Plate Chambers (RPC). The momentum resolution of the charged particles is 0.5% at 1 GeV/ c in a 1 Tesla magnetic field. The energy loss (dE/dx) measurement provided by the MDC has a resolution better than 6% for electrons from Bhabha scattering. The photon energy resolution can reach 2.5% (5%) at 1 GeV in the barrel (endcaps) of the EMC. And the time resolution of the TOF is 80 ps in the barrel and 110 ps in the endcaps.

Monte Carlo (MC) simulated events are used to determine the detection efficiency, optimize the selection criteria, and study the possible backgrounds. The simulation of the BESIII detector is based on GEANT4 [11], in which the interactions of the particles with the detector material are simulated. The $\psi(3686)$ resonance is produced with KKMC [12], which

155 is the event generator based on precise predictions of the Electroweak Standard Model for
 156 the process $e^+e^- \rightarrow f\bar{f} + n\gamma$, where $f = e, \mu, \tau, d, u, s, c, b$, and n is an integer number.
 157 The subsequent decays are generated with EVTGEN [13]. The study of the background is
 158 based on a sample of 10^8 $\psi(3686)$ inclusive decays, generated with known branching fractions
 159 taken from the Particle Data Group (PDG) [5], or with LUNDCHARM [14] for the unmeasured
 160 decays.

161 III. EVENT SELECTION

162 The decays of $\psi(3686) \rightarrow \gamma\eta_c(2S)$ with $\eta_c(2S) \rightarrow K_S^0 K^\pm \pi^\mp \pi^+ \pi^-$ are selected for this
 163 analysis. A charged track should have good quality in the track fitting and be within the
 164 angle coverage of the MDC, $|\cos\theta| < 0.93$. A good charged track (excluding those from
 165 K_S^0 decays) is required to pass within 1 cm of the e^+e^- annihilation interaction point (IP)
 166 in the transverse direction to the beam line and within 10 cm of the IP along the beam
 167 axis. Charged-particle identification (PID) is based on combining the dE/dx and TOF
 168 information to the variable $\chi_{\text{PID}}^2(i) = \left(\frac{dE/dx_{\text{measured}} - dE/dx_{\text{expected}}}{\sigma_{dE/dx}}\right)^2 + \left(\frac{\text{TOF}_{\text{measured}} - \text{TOF}_{\text{expected}}}{\sigma_{\text{TOF}}}\right)^2$.
 169 The values $\chi_{\text{PID}}^2(i)$ and the corresponding confidence levels $\text{Prob}_{\text{PID}}(i)$ are calculated for
 170 each charged track for each particle hypothesis i (pion, kaon, or proton).

171 Photon candidates are required to have energy greater than 25 MeV in the EMC both
 172 for the barrel region ($|\cos\theta| < 0.8$) and the endcap region ($0.86 < |\cos\theta| < 0.92$). In order
 173 to improve the reconstruction efficiency and the energy resolution, the energy deposited in
 174 the nearby TOF counter is included. EMC timing requirements are used to suppress noise
 175 and remove energy deposits unrelated to the event. Candidate events must have exactly six
 176 charged tracks with net charge zero and at least one good photon.

177 K_S^0 candidates are reconstructed from secondary vertex fits to all the oppositely charged-
 178 track pairs in an event (assuming the tracks to be π^\pm). The combination with the best fit
 179 quality is kept for further analysis, where the K_S^0 candidate must have an invariant mass
 180 within 10 MeV/ c^2 of the K_S^0 nominal mass and the secondary vertex is well separated from
 181 the interaction point. At least one good K_S^0 is reconstructed, and the related information is
 182 used as input for the subsequent kinematic fit.

183 After tagging the $\pi^+\pi^-$ pair from the K_S^0 , the other charged particles should be three
 184 pions and one kaon. To decide the species of those particles, we make four different particle
 185 combination assumptions: $K^+\pi^-\pi^+\pi^-$, $\pi^+K^-\pi^+\pi^-$, $\pi^+\pi^-K^+\pi^-$, and $\pi^+\pi^-\pi^+K^-$. For
 186 the different assumptions, four-momentum conservation constraints (4C) are required to
 187 be satisfied for each event candidate. For each event, the M1-photon is selected with the
 188 minimum chi-square of the 4C kinematic fit (χ_{4C}^2) by looping over all the good photons. Then
 189 the χ_{4C}^2 and the chi-squares of the particle-identification for kaon (χ_K^2) and pions (χ_π^2) are
 190 added together as the total chi-square (χ_{total}^2) for event selection. The types of particles are
 191 determined by choosing the smallest total chi-square. Events with $\chi_{\text{total}}^2 < 60$ are accepted
 192 as the $\gamma K_S^0 K^\pm \pi^\mp \pi^+ \pi^-$ candidates.

193 To suppress the $\psi(3686) \rightarrow \pi^+\pi^- J/\psi$, $J/\psi \rightarrow \gamma K_S^0 K^\pm \pi^\mp$ decay, events are rejected
 194 if the recoil mass of any $\pi^+\pi^-$ pair is within 15 MeV/ c^2 of the J/ψ nominal mass. The
 195 $\psi(3686) \rightarrow \eta J/\psi$, $\eta \rightarrow \gamma\pi^+\pi^-$ events are rejected if the mass of $K_S^0 K^\pm \pi^\mp$ is greater than
 196 3.05 GeV/ c^2 . In order to suppress $\psi(3686) \rightarrow \eta' K_S^0 K^\pm \pi^\mp$, $\eta' \rightarrow \gamma\pi^+\pi^-$ decays, events are
 197 removed if the mass of any $\gamma\pi^+\pi^-$ combination is within 20 MeV/ c^2 of the nominal η' mass.

198 **IV. DATA ANALYSIS**

199 The results of an analysis of the inclusive MC data sample showed that the primary
 200 source of background is $\psi(3686) \rightarrow K_S^0 K^\pm \pi^\mp \pi^+ \pi^-$. There are two mechanisms for this de-
 201 cay to produce background: a fake photon, or a photon from final-state radiation (FSR) is
 202 incorporated into the final state. Other backgrounds include $\psi(3686) \rightarrow \pi^0 K_S^0 K^\pm \pi^\mp \pi^+ \pi^-$
 203 with a missing photon and initial state radiation (ISR). The phase space process $\psi(3686) \rightarrow$
 204 $\gamma K_S^0 K^\pm \pi^\mp \pi^+ \pi^-$ has the same final states as our signal, so it should be considered as an ir-
 205 reducible background. As discussed in a later section, the size of this irreducible background
 206 is estimated using a region of $K_S^0 K^\pm \pi^\mp \pi^+ \pi^-$ mass away from the $\eta_c(2S)$ mass.

207 In the $\psi(3686) \rightarrow K_S^0 K^\pm \pi^\mp \pi^+ \pi^-$ background with a fake photon, a peak could be pro-
 208 duced in the $K_S^0 K^\pm \pi^\mp \pi^+ \pi^-$ mass spectrum close to the expected $\eta_c(2S)$ mass with a sharp
 209 cutoff due to the 25 MeV photon energy threshold. Considering that the fake photon does
 210 not contribute useful information to the kinematic fit, we set the photon energy free in the
 211 kinematic fit to avoid the mass distortion caused by the 25 MeV photon energy threshold.
 212 We call this the 3C kinematic fit and produce the mass spectrum based on it. MC studies
 213 demonstrate that with the 3C kinematic fit, the energy of the fake photon tends to zero,
 214 which is helpful in separating the signal from the fake photon background, as shown in
 Fig 1 [16].

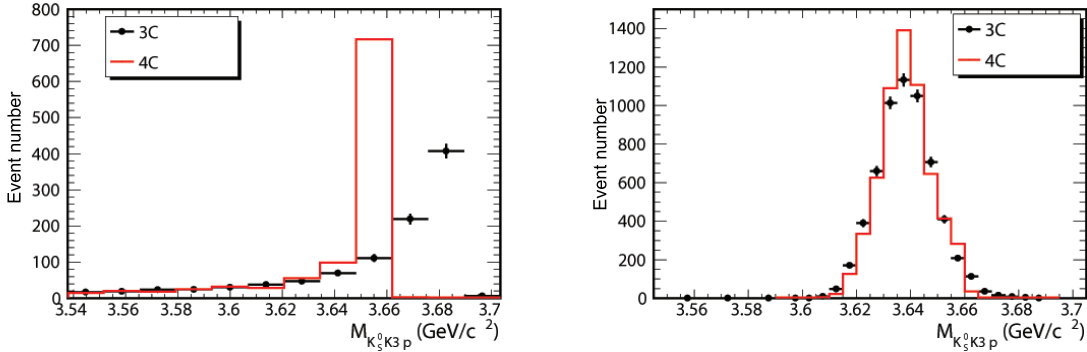


FIG. 1: Invariant mass spectrum of $K_S^0 K^\pm \pi^\mp \pi^+ \pi^-$ for the background $\psi(3686) \rightarrow K_S^0 K^\pm \pi^\mp \pi^+ \pi^-$ with a fake photon (left panel) and the signal $\psi(3686) \rightarrow \gamma \eta_c(2S), \eta_c(2S) \rightarrow K_S^0 K^\pm \pi^\mp \pi^+ \pi^-$ (right panel). The points with error bars are 3C kinematic fit results, and the solid lines are 4C kinematic fit results.

215 In the other $\psi(3686) \rightarrow K_S^0 K^\pm \pi^\mp \pi^+ \pi^-$ background, a photon from final state radi-
 216 ation (γ_{FSR}) could contaminate our signal. The $M_{K_S^0 K^\pm \pi^\mp \pi^+ \pi^-}^{3C}$ with the FSR process has a
 217 long tail from 3.58 GeV/c^2 to 3.68 GeV/c^2 in our $\eta_c(2S)$ signal region. We have to es-
 218 timate the contribution of this FSR process, because it contributes to the background in
 219 our signal region and cannot be reduced for the same final states as the signal. FSR is
 220 simulated in our MC generated data with PHOTOS [15], and the FSR contribution is
 221 scaled by the ratio of FSR fractions in data and MC generated data for a control sample
 222 of $\psi(3686) \rightarrow \gamma \pi^+ \pi^- K^+ K^-$ and $\psi(3686) \rightarrow \gamma \pi^+ \pi^- \pi^+ \pi^-$ [16]. The background contribu-
 223 tions from $\psi(3686) \rightarrow K_S^0 K^\pm \pi^\mp \pi^+ \pi^-$ with fake photons and γ_{FSR} are estimated with MC
 224 distributions normalized according to branching ratios we measured.
 225

226 The channel $\psi(3686) \rightarrow \pi^0 K_S^0 K^\pm \pi^\mp \pi^+ \pi^-$ can contaminate our signal when one of
 227 the photons from the π^0 is not detected. MC generated events of the $\psi(3686) \rightarrow$
 228 $\pi^0 K_S^0 K^\pm \pi^\mp \pi^+ \pi^-$ process, based on the phase space model, and which satisfy the selec-
 229 tion criteria for the $\psi(3686) \rightarrow \gamma K_S^0 K^\pm \pi^\mp \pi^+ \pi^-$ signal, are taken to study this background
 230 and estimate its response. To prove the correctness of the MC simulation, the $\psi(3686) \rightarrow$
 231 $\pi^0 K_S^0 K^\pm \pi^\mp \pi^+ \pi^-$ control sample, which is selected from the colliding data, times the effi-
 232 ciency to reconstruct $\psi(3686) \rightarrow \pi^0 K_S^0 K^\pm \pi^\mp \pi^+ \pi^-$ events as $\psi(3686) \rightarrow \gamma K_S^0 K^\pm \pi^\mp \pi^+ \pi^-$ is
 233 shown in Fig. 2 and compared with the same distribution obtained from the corresponding
 234 $\psi(3686) \rightarrow \pi^0 K_S^0 K^\pm \pi^\mp \pi^+ \pi^-$ MC simulation. The consistency of the two distributions is
 235 checked by the Kolmogorov-Smirnov test [17], and a good agreement is verified (the consis-
 236 tency probability reaches 0.28).

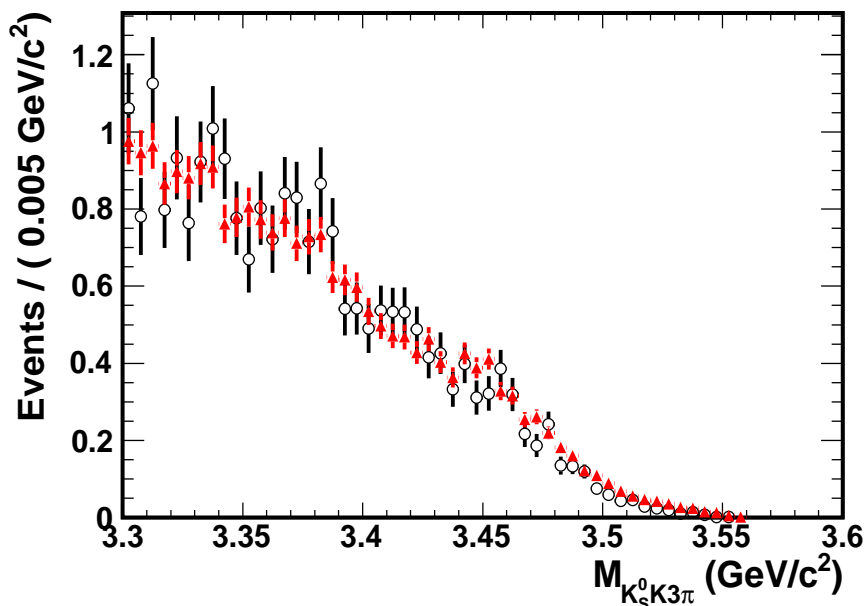


FIG. 2: The invariant mass distribution of $K_S^0 K 3\pi$ for the background from $\psi(3686) \rightarrow$
 $\pi^0 K_S^0 K^\pm \pi^\mp \pi^+ \pi^-$. The black circles with error bars show the background shape obtained from
 the collider data. The red triangles with error bars represent the $M_{K_S^0 K 3\pi}$ distribution from a
 corresponding MC sample.

237 The background from the continuum (including ISR) is estimated with collider data
 238 taken at a center of mass energy of 3.65 GeV. The events must pass the signal selection
 239 requirements and are then normalized according to differences in integrated luminosity and
 240 cross section. Particle momenta and energies are scaled to account for the beam-energy
 241 difference. The resultant number and the $K_S^0 K 3\pi$ invariant mass shape considering these
 242 scale factors ($f_{\text{continuum}} = 3.6$) are used in the final fit.

243 The background from phase space has the same final states as the signal. To select a
 244 clean phase space sample, the $M_{K_S^0 K 3\pi}$ region [3.20, 3.30] GeV/c^2 is chosen. This choice is
 245 made because there is a long η_c tail in the area $M_{K_S^0 K 3\pi} < 3.0 \text{ GeV}/c^2$ which originates from
 246 the decay channel $\psi(3686) \rightarrow \gamma \eta_c$. There are three obvious peaks in the area $M_{K_S^0 K 3\pi} >$

247 $3.3 \text{ GeV}/c^2$ which are from the decay channel $\psi(3686) \rightarrow \gamma\chi_{cJ}, (J = 0, 1, \text{ and } 2)$. The
 248 branching fraction of the phase space process is calculated to be 1.73×10^{-4} . The $K_S^0 K 3\pi$
 249 invariant mass spectrum of MC phase space events is used in the final fit, while the number
 250 of events is left floating. The number of phase space events obtained by fitting the mass
 251 spectrum is consistent with that estimated by the branching fraction we calculated.

252 In the $K_S^0 K 3\pi$ mass spectrum fitting, the fitting range is from $3.30 \text{ GeV}/c^2$ to $3.70 \text{ GeV}/c^2$
 253 so that the contributions of backgrounds and $\chi_{cJ} (J = 0, 1, \text{ and } 2)$ can be taken into account.
 254 The final mass spectrum and the fitting results are shown in Fig. 3. The fitting function
 255 consists of the following components: $\eta_c(2S)$, $\chi_{cJ} (J = 0, 1, \text{ and } 2)$ signals and $\psi(3686) \rightarrow$
 $K_S^0 K^\pm \pi^\mp \pi^+ \pi^-$, $\psi(3686) \rightarrow \pi^0 K_S^0 K^\pm \pi^\mp \pi^+ \pi^-$, ISR, and phase space backgrounds. The line

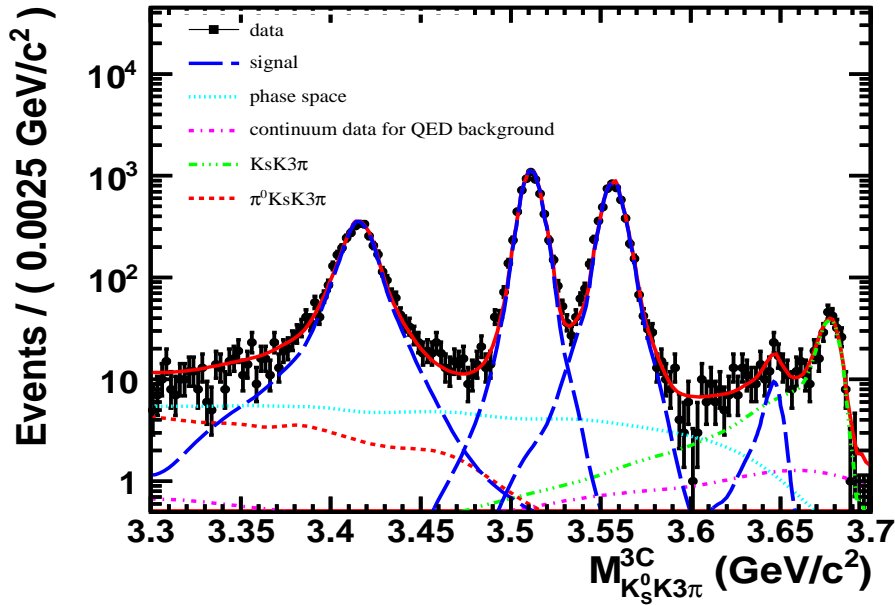


FIG. 3: The results of fitting the mass spectrum for χ_{cJ} and $\eta_c(2S)$. The black dots are the collider data, the blue long-dashed line shows the χ_{cJ} and $\eta_c(2S)$ signal shapes, the cyan dotted line represents the phase space contribution, the violet dash-dotted line shows the continuum data contribution, the green dash-double-dotted line shows the contribution of $\psi(3686) \rightarrow K_S^0 K^\pm \pi^\mp \pi^+ \pi^-$, and the red dashed line is the contribution of $\psi(3686) \rightarrow \pi^0 K_S^0 K^\pm \pi^\mp \pi^+ \pi^-$.

256 shapes for χ_{cJ} are obtained from MC simulations. These can describe the χ_{cJ} spectrum
 257 well in the collider data after applying the kinematic fit correction [18]. The line shape for
 258 $\eta_c(2S)$ produced by such a M1 transition is given by:

$$(E_\gamma^3 \times BW(m) \times \text{damping}(E_\gamma)) \otimes \text{Gauss}(0, \sigma), \quad (1)$$

260 where $BW(m)$ is the Breit-Wigner function, m is the invariant mass of $K_S^0 K 3\pi$, $E_\gamma =$
 261 $\frac{m_\psi(3686)^2 - m^2}{2m_\psi(3686)}$ is the energy of the transition photon in the rest frame of $\psi(3686)$, $\text{damping}(E_\gamma)$
 262 is the function to damp the diverging tail raised by E_γ^3 and $\text{Gauss}(0, \sigma)$ is the Gaussian
 263 function describing the detector resolution. The detector resolution is determined by the

264 MC study, and the difference of data and MC has been taken into account which introduces
 265 negligible uncertainties in branching fraction, mass and width measurements comparing with
 266 other factors. The form of the damping function is somewhat arbitrary, and one suitable
 267 function used by KEDR [19] for a similar process is

$$damping(E_\gamma) = \frac{E_0^2}{E_\gamma E_0 + (E_\gamma - E_0)^2}, \quad (2)$$

268 where $E_0 = \frac{m_{\psi(3686)}^2 - m_{\eta_c(2S)}^2}{2m_{\psi(3686)}}$ is the peaking energy of the transition photon. Another damping
 269 function used by CLEO [20] is inspired by the overlap of wave functions

$$damping(E_\gamma) = \exp(-E_\gamma^2/8\beta^2), \quad (3)$$

270 with $\beta = (65.0 \pm 2.5)$ MeV from CLEO's fit. In our analysis, the KEDR function (Eq. 2) is
 271 used in the fitting to give the final results, and the CLEO one (Eq. 3) is used to estimate
 272 the possible uncertainty caused by the form of damping functions.

273 The result for the yield of $\eta_c(2S)$ events is 57 ± 17 with a significance of 4.2σ . The
 274 significance is calculated from log-likelihood differences between fits with and without the
 275 $\eta_c(2S)$ component. The robustness of this result was tested by considering different damping
 276 factor forms, FSR fractions, and background assumptions. In all the cases, the statistical
 277 significance is found to be larger than 4σ . The resulting mass and width from the fit are
 278 3646.9 ± 1.6 MeV/ c^2 and 9.9 ± 4.8 MeV/ c^2 (statistical errors only), respectively. We find
 279 the product branching fraction $\mathcal{B}(\psi(3686) \rightarrow \gamma\eta_c(2S)) \times \mathcal{B}(\eta_c(2S) \rightarrow K_S^0 K^\pm \pi^\mp \pi^+ \pi^-) =$
 280 $(7.03 \pm 2.10) \times 10^{-6}$ with the efficiency of 11.1% for the signal selection.

281 V. ESTIMATION OF SYSTEMATIC UNCERTAINTIES

282 The systematic uncertainties in the $\eta_c(2S)$ mass and width measurements are estimated
 283 by the uncertainties in the damping factor, scale factor and the number of $\psi(3686) \rightarrow$
 284 $\pi^0 K_S^0 K^\pm \pi^\mp \pi^+ \pi^-$ events. The results are summarized in Table I, and described in more
 285 detail in the following.

TABLE I: Uncertainties in the mass and width of $\eta_c(2S)$.

Source	mass uncertainty	width uncertainty
Damping factor	< 0.1%	28%
Scale factor	negligible	5%
No. of $\pi^0 K_S^0 K^\pm \pi^\mp \pi^+ \pi^-$	< 0.1%	5%
Total	< 0.1%	29%

286 We change the damping factor to the CLEO form, then compare the results with that
 287 obtained with the KEDR form, and the difference is taken as the uncertainty originating from
 288 the damping factor. The background shape of $\psi(3686) \rightarrow K_S^0 K^\pm \pi^\mp \pi^+ \pi^-$ could influence the
 289 fitting results, so we change the FSR scale factor of 1.46 by 1σ to 1.412 and 1.504, and the
 290 difference in the results is taken as the uncertainty coming from scale factor. In the fitting

291 of the mass spectrum, the number of events for $\psi(3686) \rightarrow \pi^0 K_S^0 K^\pm \pi^\mp \pi^+ \pi^-$ is fixed. We
 292 change the number of events by 1σ , and take the difference in the results as the uncertainty
 293 originating from the number of background events from $\psi(3686) \rightarrow \pi^0 K_S^0 K^\pm \pi^\mp \pi^+ \pi^-$ events.

294 The systematic errors in the measurement of the branching fraction are summarized in
 295 Table II and explained below.

TABLE II: Summary of systematic uncertainties in the measurement of $\mathcal{B}(\psi(3686) \rightarrow \gamma \eta_c(2S), \eta_c(2S) \rightarrow K_S^0 K^\pm \pi^\mp \pi^+ \pi^-)$.

Sources	Systematic uncertainties
MDC tracking	4%
Photon reconstruction	1%
K_S^0 reconstruction	4%
Kinematic fitting and PID	2%
Total number of $\psi(3686)$	0.8%
Damping factor	2%
Scale factor	5%
No. of $\psi(3686) \rightarrow \pi^0 K_S^0 K^\pm \pi^\mp \pi^+ \pi^-$	2%
$\eta_c(2S)$ width	3%
Intermediate states	5%
Total	10%

296 The tracking efficiencies for K^\pm and π^\pm as functions of transverse momentum have been
 297 studied with the process $J/\psi \rightarrow K_S^0 K^\pm \pi^\mp$, $K_S^0 \rightarrow \pi^+ \pi^-$ and $\psi(3686) \rightarrow \pi^+ \pi^- J/\psi$, respec-
 298 tively. The efficiency difference between data and MC is 1% for each K^\pm track or π^\pm track
 299 [21, 22]. So the uncertainty of the tracking efficiency is 4% for four charged tracks. The
 300 uncertainty of the two pions from K_S^0 is not included here, because it is included in the K_S^0
 301 uncertainty.

302 The uncertainty due to photon reconstruction is 1% per photon [23]. This is determined
 303 from studies of photon detection efficiencies in the process $J/\psi \rightarrow \rho^0 \pi^0$, $\rho^0 \rightarrow \pi^+ \pi^-$ and
 304 $\pi^0 \rightarrow \gamma \gamma$.

305 Three parts contribute to the efficiency for K_S^0 reconstruction: the geometric acceptance,
 306 tracking efficiency and the efficiency of K_S^0 selection. The first part was estimated using
 307 an MC sample, and the other two were studied by the process $J/\psi \rightarrow K^* \bar{K}^0 + c.c.$. The
 308 difference between data and MC is estimated to be 4%.

309 To estimate the uncertainty of kinematic fitting, we first correct the track helix param-
 310 eters (ϕ_0 , κ , $tg\lambda$) to reduce the difference on χ_{4C}^2 from kinematic fitting between data and
 311 MC, where ϕ_0 is the azimuthal angle specifies the pivot with respect to the helix center, κ is
 312 the reciprocal of the transverse momentum and $tg\lambda$ is the slope of the track. The correction
 313 factors are obtained from $J/\psi \rightarrow \phi f_0(980)$, $\phi \rightarrow K^+ K^-$ and $f_0(980) \rightarrow \pi^+ \pi^-$. The MC
 314 samples after correction are used to estimate the efficiency and fit the invariant mass spec-
 315 trum. Fig. 4 (left) shows the χ_{4C+PID}^2 distribution with and without the correction in MC
 316 and in data. The distribution of χ_{4C+PID}^2 with correction is closer to the data than without
 317 correction. However, the agreement is not perfect, and we take the systematic uncertainty
 318 to be the difference of the efficiency between MC before and after correction [18]. The com-

319 parison is shown in Fig. 4 (right). The systematic uncertainty from kinematic fitting is 2%
 320 with $\chi_{4C+PID}^2 < 60$.

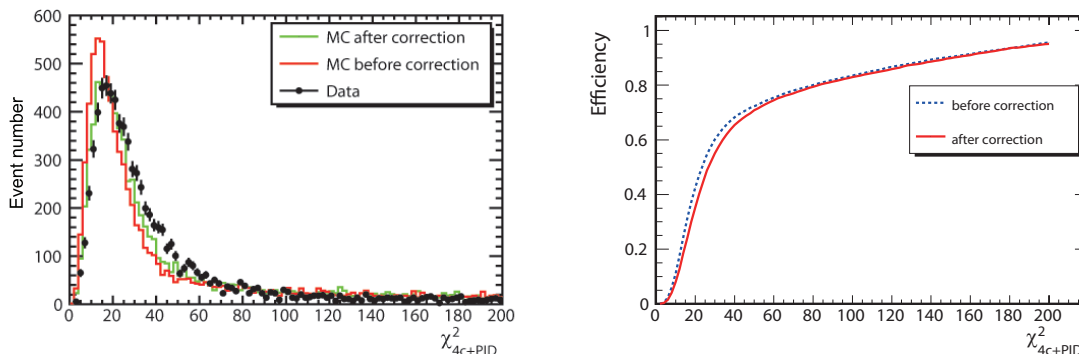


FIG. 4: [left panel] The χ_{4C+PID}^2 distribution with and without the correction in MC and in data. The black dots show the distribution of χ_{4C+PID}^2 in the data, the orange (green) histogram represents the distributions of χ_{4C+PID}^2 without (with) correction in MC. [right panel] Efficiency results with and without correction at different χ_{4C+PID}^2 cuts.

321 We also change the form of the damping factor, the value of the FSR scale factor and
 322 the number of events for $\psi(3686) \rightarrow \pi^0 K_S^0 K^\pm \pi^\mp \pi^+ \pi^-$ to estimate the uncertainties in the
 323 branching fraction, which is the same as the method to estimate the uncertainties of $\eta_c(2S)$
 324 mass and width. The total number of $\psi(3686)$ events is estimated by the inclusive hadronic
 325 events, and the uncertainty is 0.8% [9].

326 To estimate the uncertainty due to the $\eta_c(2S)$ width, we change the $\eta_c(2S)$ width of
 327 9.9 MeV/ c^2 by 1σ to 5.1 MeV/ c^2 and 14.7 MeV/ c^2 in the MC simulation. Comparing
 328 the efficiencies with 11.1%, which is used in calculating the branching fraction, we find a
 329 difference of 3%.

330 For the uncertainty from intermediate states, we generate MC samples including these
 331 states ($K^*(892)$, ρ) and compare the corresponding efficiencies. We take the 5% difference
 332 as the uncertainty.

333 We assume that all the sources of systematic uncertainties are independent and the overall
 334 systematic uncertainties are obtained by adding all single ones in quadrature.

335 VI. CONCLUSION

336 We observe the decay mode $\eta_c(2S) \rightarrow K_S^0 K^\pm \pi^\mp \pi^+ \pi^-$ and establish the M1 transition
 337 of $\psi(3686) \rightarrow \gamma \eta_c(2S)$ using this decay mode. The mass of the $\eta_c(2S)$ is measured to be
 338 $3646.9 \pm 1.6(\text{stat}) \pm 3.6(\text{syst})$ MeV/ c^2 , and the width is $9.2 \pm 4.8(\text{stat}) \pm 2.9(\text{syst})$ MeV.
 339 Comparing with BESIII previous measurements [8], the width is consistent with each other
 340 within 1 standard deviation and the mass is about 2 standard deviation. The product
 341 branching fraction is measured to be $\mathcal{B}(\psi(3686) \rightarrow \gamma \eta_c(2S)) \times \mathcal{B}(\eta_c(2S) \rightarrow K_S^0 K^\pm \pi^\mp \pi^+ \pi^-)$
 342 $= (7.03 \pm 2.10(\text{stat}) \pm 0.70(\text{syst})) \times 10^{-6}$. The statistical significance is greater than 4
 343 standard deviation.

344 To compare with the BABAR results [6],

$$\frac{\mathcal{B}(\eta_c(2S) \rightarrow K^+ K^- \pi^+ \pi^- \pi^0)}{\mathcal{B}(\eta_c(2S) \rightarrow K_S^0 K^\pm \pi^\mp)} = 2.2 \pm 0.5 \pm 0.5, \quad (4)$$

345 we take the value of $(4.31 \pm 0.75) \times 10^{-6}$ as measured by BESIII for $\mathcal{B}(\psi(3686) \rightarrow \gamma \eta_c(2S)) \times$
 346 $\mathcal{B}(\eta_c(2S) \rightarrow K_S^0 K^\pm \pi^\mp)$ [8], and assuming that

$$\frac{\mathcal{B}(\eta_c(2S) \rightarrow K^+ K^- \pi^+ \pi^- \pi^0)}{\mathcal{B}(\eta_c(2S) \rightarrow K_S^0 K^\pm \pi^\mp \pi^+ \pi^-)} = 1.52, \quad (5)$$

347 where the value 1.52 is calculated in χ_{cJ} decays, which has the same isospin, we obtain

$$\frac{\mathcal{B}(\eta_c(2S) \rightarrow K^+ K^- \pi^+ \pi^- \pi^0)}{\mathcal{B}(\eta_c(2S) \rightarrow K_S^0 K^\pm \pi^\mp)} = 1.52 \cdot \frac{\mathcal{B}(\eta_c(2S) \rightarrow K_S^0 K^\pm \pi^\mp \pi^+ \pi^-)}{\mathcal{B}(\eta_c(2S) \rightarrow K_S^0 K^\pm \pi^\mp)} = 2.48 \pm 0.56 \pm 0.33. \quad (6)$$

348 These two results are consistent with each other after considering the statistical and sys-
 349 tematic uncertainties.

350 Acknowledgments

351 The BESIII collaboration is grateful to the staff of BEPCII and the computing center
 352 for their tireless efforts. This work is supported in part by the Ministry of Science and
 353 Technology of China under Contract No. 2009CB825200; National Natural Science Foun-
 354 dation of China (NSFC) under Contracts Nos. 10625524, 10821063, 10825524, 10835001,
 355 10935007, 11125525, 11235011, 10979038, 11079030, 11005109, 11275189, U1232201; Joint
 356 Funds of the National Natural Science Foundation of China under Contracts Nos. 11079008,
 357 11179007; the Chinese Academy of Sciences (CAS) Large-Scale Scientific Facility Program;
 358 CAS under Contracts Nos. KJCX2-YW-N29, KJCX2-YW-N45; 100 Talents Program of
 359 CAS; the Fundamental Research Funds for the Central Universities under Contracts No.
 360 2030040126, China; German Research Foundation DFG under Contract No. Collaborative
 361 Research Center CRC-1044; Istituto Nazionale di Fisica Nucleare, Italy; Ministry of De-
 362 velopment of Turkey under Contract No. DPT2006K-120470; U. S. Department of Energy
 363 under Contracts Nos. DE-FG02-04ER41291, DE-FG02-94ER40823, DE-FG02-05ER41374;
 364 U.S. National Science Foundation; University of Groningen (RuG); the Helmholtzzentrum
 365 für Schwerionenforschung GmbH (GSI), Darmstadt; and WCU Program of National Re-
 366 search Foundation of Korea under Contract No. R32-2008-000-10155-0.

-
- 367 [1] S. K. Choi *et al.* (BELLE Collaboration), Phys. Rev. Lett. **89**, 102001 (2002).
 368 [2] D. M. Asner *et al.* (CLEO Collaboration), Phys. Rev. Lett. **92**, 142001 (2004).
 369 [3] B. Aubert *et al.* (BABAR Collaboration), Phys. Rev. Lett. **92**, 142002 (2004).
 370 [4] B. Aubert *et al.* (BABAR Collaboration), Phys. Rev. Lett. **96**, 052002 (2006).
 371 [5] J. Beringer *et al.*, Phys. Rev. D **86**, 010001 (2012).
 372 [6] P. del Amo Sanchez *et al.* (BABAR Collaboration), Phys. Rev. D **84**, 012004 (2011).
 373 [7] Softley, Atomic Spectra, Oxford: Oxford University Press, ISBN 0-19-855688-8 (1994).
 374 [8] M. Ablikim *et al.* (BESIII Collaboration), Phys. Rev. Lett. **109**, 042003 (2012).

- 375 [9] M. Ablikim *et al.* (BESIII Collaboration), arXiv:1209.6199[hep-ex].
376 [10] M. Ablikim *et al.* (BESIII Collaboration), Nucl. Instrum. Meth. A **614**, 345 (2010).
377 [11] S. Agostinelli *et al.* (GEANT4 Collaboration), Nucl. Instrum. Meth. A **506**, 250 (2003).
378 [12] S. Jadach, B. F. L. Ward and Z. Was, Comp. Phys. Commu. **130**, 260 (2000); Phys. Rev. D
379 **63**, 113009 (2001).
380 [13] <http://www.slac.stanford.edu/~lange/EvtGen/>; R. G. Ping *et al.*, Chinese Physics C **32**, 599
381 (2008).
382 [14] J. C. Chen *et al.*, Phys. Rev. D **62**, 034003 (2000).
383 [15] E. Barberio and Z. Was, Comput. Phys. Commun. **79**, 291 (1994).
384 [16] M. Ablikim *et al.* (BESIII Collaboration), Phys. Rev. D **84**, 091102 (2011).
385 [17] Kolmogorov A, G. Inst. Ital. Attuari **4**, 83 (1933).
386 [18] M. Ablikim *et al.* (BESIII Collaboration), arXiv:1208.4805[hep-ex].
387 [19] V. V. Anashin *et al.*, arXiv:1012.1694[hep-ex].
388 [20] R. E. Mitchell *et al.* (CLEO Collaboration), Phys. Rev. Lett. **102**, 011801 (2009).
389 [21] M. Ablikim *et al.* (BESIII Collaboration), Phys. Rev. Lett. **107**, 092001 (2011).
390 [22] M. Ablikim *et al.* (BESIII Collaboration), Phys. Rev. D **83**, 112005 (2011).
391 [23] M. Ablikim *et al.* (BESIII Collaboration), Phys. Rev. D **81**, 052005(2010).